Antiviral Research 171 (2019) 104592

Contents lists available at ScienceDirect

Antiviral Research

journal homepage: www.elsevier.com/locate/antiviral

Cholesterol-conjugated stapled peptides inhibit Ebola and Marburg viruses *in vitro* and *in vivo*

Antonello Pessi[a], Sandra L. Bixler[b,c], Veronica Soloveva[b,c,1], Sheli Radoshitzky[b,c], Cary Retterer[b], Tara Kenny[b], Rouzbeh Zamani[b], Glenn Gomba[b], Dima Gharabeih[b], Jay Wells[b], Kelly S. Wetzel[b], Travis K. Warren[b,c], Ginger Donnelly[b], Sean A. Van Tongeren[b], Jesse Steffens[b], Allen J. Duplantier[b,c], Christopher D. Kane[b,c,**], Pascale Vicat[d], Valerie Couturier[d], Kent E. Kester[e], John Shiver[e], Kara Carter[f,2], Sina Bavari[b,*]

[a] *PeptiPharma, Rome, Italy*
[b] *United States Army Medical Research Institute of Infectious Diseases (USAMRIID), 1425 Porter Street, Frederick, MD, 21702, USA*
[c] *Therapeutic Development Center, USAMRIID, Frederick, MD, 21702, USA*
[d] *Sanofi, Paris, France*
[e] *Sanofi Pasteur, Swiftwater, PA, USA*
[f] *Sanofi, Cambridge, MA, USA*

ARTICLE INFO

Keywords:
Ebola virus
Therapeutic
Peptides
Cholesterol
Rodents

ABSTRACT

Filoviridae currently includes five official and one proposed genera. Genus *Ebolavirus* includes five established and one proposed ebolavirus species for Bombali virus (BOMV), Bundibugyo virus (BDBV), Ebola virus (EBOV), Reston virus (RESTV), Sudan virus (SUDV) and Taï Forest virus (TAFV), and genus *Marburgvirus* includes a single species for Marburg virus (MARV) and Ravn virus (RAVV). Ebola virus (EBOV) has emerged as a significant public health concern since the 2013–2016 Ebola Virus Disease outbreak in Western Africa. Currently, there are no therapeutics approved and the need for Ebola-specific therapeutics remains a gap. In search for anti-Ebola therapies we tested the idea of using inhibitory properties of peptides corresponding to the C-terminal heptad-repeat (HR2) domains of class I fusion proteins against EBOV infection. The fusion protein GP_2 of EBOV belongs to class I, suggesting that a similar strategy to HIV may be applied to inhibit EBOV infection. The serum half-life of peptides was expanded by cholesterol conjugation to allow daily dosing. The peptides were further constrained to stabilize a helical structure to increase the potency of inhibition. The EC_{50}s of lead peptides were in low micromolar range, as determined by a high-content imaging test of EBOV-infected cells. Lead peptides were tested in an EBOV lethal mouse model and efficacy of the peptides were determined following twice-daily administration of peptides for 9 days. The most potent peptide was able to protect mice from lethal challenge of mouse-adapted Ebola virus. These data show that engineered peptides coupled with cholesterol can inhibit viral production, protect mice against lethal EBOV infection, and may be used to build novel therapeutics against EBOV.

1. Introduction

The *Filoviridae* family consists of five genera. The most recognized *Ebolavirus* genus consists of five established species Ebola Zaire (EBOV), Sudan (SUDV), Bundibugyo (BDBV), Reston (RESTV), and Taï Forest (TAFV) viruses (Kuhn et al., 2014a, 2014b). Marburgvirus and ebolaviruses have caused human epidemics of viral hemorrhagic fever, with high case fatality rates (Feldmann and Geisbert, 2011). The majority of outbreaks are due to EBOV. Since the first recognized outbreak in 1976, numerous Ebola virus disease outbreaks have occurred over the years, but until the catastrophic West Africa epidemic fewer than 2500 cases have been reported altogether (Haque et al., 2015). The

* Corresponding author. US Army Medical Research Institute of Infectious Diseases (USAMRIID), 1425 Porter Street, Ft. Detrick, MD, 21702, USA.
** Corresponding author. US Army Medical Research Institute of Infectious Diseases (USAMRIID), 1425 Porter Street, Ft. Detrick, MD, 21702, USA.
E-mail addresses: christopher.d.kane.civ@mail.mil (C.D. Kane), sina.bavari.civ@mail.mil (S. Bavari).
[1] Merck Research Laboratories, Cambridge, MA, USA.
[2] Evotec SE, Manfred Eigen Campus, Essener Bogen 7, 22419, Hamburg, Germany.

https://doi.org/10.1016/j.antiviral.2019.104592
Received 9 June 2019; Received in revised form 22 August 2019; Accepted 25 August 2019
Available online 29 August 2019

2013–2016 epidemic resulted in approximately 28,200 cases and 11,300 deaths (Holmes et al., 2016). Although the epidemic has now subsided, the increase in outbreak frequency, number of cases, and associated social and economic cost highlights the need for development and rapid evaluation of pre- and post-exposure treatments (Cross et al., 2018; Haque et al., 2015). Extraordinary efforts to field-test an experimental Ebola vaccine in the outbreak setting have produced positive results (Skrip and Galvani, 2016). Several small molecule and antibody therapies have also provided promising preclinical outcomes using filovirus non-human primate and other animal models (Bixler et al., 2018; Bornholdt et al., 2016; Flyak et al., 2016; Frei et al., 2016; Furuyama et al., 2016; Misasi et al., 2016; Nyakatura et al., 2015; Qiu et al., 2016; Warren et al., 2014, 2016; Wec et al., 2016). Uptake inhibitors, which block virus entry, could be used in combination with these therapeutics to improve efficacy and/or reduce the potential for development of antiviral drug resistance. However, parallel efforts towards antiviral entry inhibitors are less advanced (Haque et al., 2015) and the need for Ebola virus-specific therapeutics remains pressing (Cross et al., 2018).

Ebola virions are enveloped and filamentous, and contain a negative-strand RNA genome. Infection requires fusion of the host and viral membranes for delivery of the viral genomic material into the cytoplasm. This process is thought to occur in host endosomal compartments and is mediated by the transmembrane glycoprotein subunit 2 (GP_2). In the pre-fusion state, the GP spike assembly consists of three copies each of the surface subunit (GP_1) and the transmembrane subunit (GP_2). Following cell attachment via GP_1, EBOV particles are internalized by micropinocytosis and the virus traffics through the endocytic pathway (Mulherkar et al., 2011; Nanbo et al., 2010; Saeed et al., 2010). There, proteolytic cleavage of GP_1 by host proteases, cysteine cathepsins, removes the C-terminal glycan cap and mucin domain sequences (Chandran et al., 2005) and exposes a receptor-binding domain (RBD). The RBD then interacts with Niemann-Pick C1 (NPC1), an obligate intracellular filovirus receptor, prior to fusion of the viral and host membranes (Carette et al., 2011; Cote et al., 2011).

EBOV GP_2 is a 'class I' fusion protein based on its two heptad repeat (HR) regions, HR1 at the N terminus and HR2 at the C terminus (Gallaher, 1996). These α-helical major domains are connected by a linker and an internal fusion loop. In the pre-fusion conformation, GP_2 forms a trimer intimately associated with GP_1 (Lee et al., 2008), in which GP_2's N-terminal HR1 and internal fusion loop pack against an adjacent GP_1 monomer. In contrast, in the post-fusion conformation the N-terminal HR1 and fusion loop of GP_2 are juxtaposed to its C-terminal HR2 in a hairpin conformation termed a 6-helix bundle (6HB) (Malashkevich et al., 1999; Weissenhorn et al., 1998).

Peptides corresponding to the C-terminal heptad-repeat (HR2) domains of class I fusion proteins are well known inhibitors of viral fusion (Eckert and Kim, 2001), with one such peptide (enfuvirtide, Fuzeon®, Roche) currently in clinical use for human immunodeficiency virus (HIV) (LaBonte et al., 2003). Enfuvirtide and other HR2 peptides inhibit membrane fusion by competing with the endogenous HR2 for binding to the N-terminal HR1, thus preventing formation of the 6HB that drives apposition of the viral and cell membranes to form the fusion pore (Eckert and Kim, 2001). The crystal structure of EBOV GP_2 in the post-fusion conformation has been determined (Malashkevich et al., 1999; Weissenhorn et al., 1998), and its overall similarity to the structure of HIV gp41 suggests that an analogous strategy for peptide-mediated inhibition may be applied to filoviruses. However, there are two major differences between the two viruses. First, the 6HB in the EBOV GP_2 post-fusion structure is considerably shorter than the corresponding 6HB of HIV gp41, consisting of only three α-helical turns each in the HR1 and HR2 regions of GP_2, compared to seven turns in gp41 (Harrison et al., 2011). Second, fusion of EBOV occurs in late endosomal compartments (Aman, 2016), a less favorable target site compared to HIV, which fuses with the cellular membrane at the cell surface.

Nevertheless, peptides were reported that inhibit EBOV pseudovirus infection (Higgins et al., 2013; Miller et al., 2011). Localization to endosomes was provided by conjugation of the HR2 EBOV peptide to either the arginine-rich segment from HIV-1 Tat protein, which is known to be targeted to endosomes (Miller et al., 2011), or to a cholesterol group (Higgins et al., 2013). The latter modification was shown to dramatically potentiate the activity of HR2-derived fusion inhibitors, by concentrating the peptide in lipid rafts, where EBOV fusion occurs (Ingallinella et al., 2009; Pessi, 2015). Additionally, cholesterol conjugation prolonged the half-life of the peptide in circulation by binding to serum proteins, making it suitable for once-daily administration (Ingallinella et al., 2009; Mathieu et al., 2017; Pessi, 2015; Porotto et al., 2010a; Welsch et al., 2013).

However, in the case of infectious EBOV the cholesterol-conjugated HR2 peptide inhibited the virus with high micromolar potency (Higgins et al., 2013), almost 1000-fold less than the cholesterol-conjugated HIV peptide C34-Chol (Ingallinella et al., 2009). We describe here how engineering of HR2 peptides coupled with cholesterol conjugation can yield potent inhibitors of EBOV infection *in vitro* and *in vivo*, that also demonstrate antiviral activity against the related Sudan virus (SUDV) and MARV.

2. Materials and methods

2.1. Facilities

All animal studies were performed in BSL-4 containment facilities at USAMRIID. The facility where this research was conducted is accredited by the Association for Assessment and Accreditation of Laboratory Animal Care, International and adheres to principles stated in the Guide for the Care and Use of Laboratory Animals, National Research Council, 2011.

2.2. Ethics statement

Research was conducted under IACUC-approved protocols in compliance with the Animal Welfare Act, PHS Policy, and other Federal statutes and regulations relating to animals and experiments involving animals.

2.3. Peptide synthesis

All peptides were custom-synthesized. American Peptide Company (Sunnyvale, CA, USA) synthesized peptides EBOV-1 to −6, and Bachem (Torrance, CA, USA) synthesized peptides EBOV-7 and -8, and a new batch of peptides EBOV-5 and -6 for a bridging study. The former company is now part of the latter. Purity was > 90% as assessed by analytical high performance liquid chromatography (HPLC) and identity was confirmed by amino acid analysis and liquid chromatography-mass spectrometry (LC-MS).

2.4. Cells

HeLa (CCL-2), U2OS (HTB-96), HEK 293T (CRL-11268) and BHK-21[C-13] (CCL-10) cell lines were purchased from the American Type Culture Collection. HeLa, HEK 293T and U2OS cells were cultured in T225 (Corning) flasks in Minimum Essential Medium (MEM, Corning Cellgro) supplemented with 10% fetal bovine serum (FBS, Hyclone), 1% L-glutamine, 10 mM HEPES, 1% non-essential amino acids, and 1% penicillin/streptomycin. BHK-21 cells were cultured in MEM supplemented with 10% FBS and 1% penicillin/streptomycin. Sub-confluent culture was passaged and split every 3 days, not exceeding 16–19 passages. Cells were lifted for plating in the assay plate 24 h before test using 0.25% Trypsin/0.5 mM EDTA solution.

2.5. Cell-based infection assays

Experiments with infectious viruses were performed in USAMRIID under appropriate biocontainment conditions. Virus stocks were all prepared and characterized at USAMRIID.

2.5.1. Filovirus infection assay

HeLa cells were harvested from 225T flasks and plated at 2000 cells per well in complete media in 384-well imaging plates (Aurora Black Square ULB 384 IQ-EB, 188 μm Clear Film Bottom, #1052-11130-S) at 20–24 h prior to treatment. Peptides were tested at 8 or 10 doses in triplicate starting at 100 μg/ml with a 2-fold step dilution. In a limited number of studies, 25μM peptide was used as the starting concentration with 2-fold step dilution. Each dose was added directly to the assay wells containing cells using the HP D300 digital dispenser (Hewlett Packard) from 20 mg/ml stock solution in 100% DMSO 2 h before infection. The final DMSO concentration in each well was normalized to 1%. The 16 wells in column 2 were not infected with virus and served as a 'no virus' control for further analysis of 0% infection. The 16 wells in column 3 were infected with virus but treated only with 1% DMSO to create high infection control to determine 100% virus infection. Treated assay plates were transferred to the biosafety level (BSL)-4 suite and after 2 h pre-incubation, were infected with one of three viruses: EBOV Makona at a multiplicity of infection (MOI) of 0.5, MARV Ci67 at MOI of 1 and SUDV Boniface at MOI of 0.08. The MOI was calculated based on the average doubling time for HeLa cells (16 h) and was selected to achieve 60–80% infection rate detected using high-content imaging (HCI) assay after 48 h of infection. The assay plates with virus were incubated at 37 °C with 5% CO_2 for 48 h. Infection was terminated by fixing the samples in a 10% formalin solution for at least 48 h before immunostaining.

2.5.2. Chikungunya virus infection assay

Infection with Chikungunya virus (CHIKV) strain AF15561 was done in U2OS cells plated at 3000 cells per well in complete growth media in 384-well imaging plates. The treatment of the cells with peptides was done as described above 2 h prior the infection. Treated plates were transferred to the BSL-3 suite to be infected with CHIKV at MOI of 0.5 and incubated for another 20 h. Infection was terminated by fixing the samples in a 10% formalin solution for an additional 24 h before immunostaining.

2.5.3. Mouse-adapted ebola virus infection assay

The BHK-21 Syrian golden hamster kidney cell line was used for infection with mouse-adapted EBOV/Mayinga. Cells were plated at 4000 cells per well in 384-well imaging plates and treated with peptides as described above. However, peptides were tested at 8 or 10 doses in triplicate starting at 200μg/mL with a 3-fold step dilution. Infection with mouse-adapted EBOV was performed in the BSL-4 suite at an MOI of 37 with the goal of achieving a 90% infection rate after 48 h of incubation. Infection was terminated by fixing the samples in a 10% formalin solution for an additional 48 h.

2.6. High-content imaging assay

Detection and quantification of viral infection in cultured cell lines was done using a high-content imaging (HCI) assay to measure viral antigen production after immunofluorescent labelling. The monoclonal primary antibody recognizing an epitope on the viral GP protein was diluted 1000-fold in blocking buffer (1xPBS with 3% BSA), added to each well of the assay plate, and incubated for 1 h at room temperature. The primary antibody mm6D8 was used to detect EBOV/Makona and mouse-adapted EBOV/Mayinga, mm3C10 to detect SUDV, mm9G4 to detect MARV, and mm2D21-1 to detect E2 protein of CHIKV virus. Following incubation, the primary antibody was removed and the cells were washed 3 times with 1xPBS. The secondary goat anti-mouse antibody conjugated with DyLight-488 (Thermo Fisher, #35502B) was used for labeling and was added to each well in the assay plate at a 1000-fold dilution in blocking buffer and incubated for 60 min at room temperature. The nuclei and cytoplasm were stained in the EBOV assay using Draq5 (Thermo Fisher, #62252) and diluted in 1xPBS. For enhanced detection of the cytoplasm area in SUDV, MARV and CHIKV infection assays, cells were stained with CellMask Deep Red (Invitrogen, #1932429) and nuclei with Hoechst 33342 (Life Technologies, #H3570) for another hour. Cell images were acquired using a PerkinElmer Opera confocal plate reader using a 10X air objective to collect 5 images per well. Cells were detected using nuclei signal emitting at 400 nm (Hoechst) or at 640 nm (Draq5). The cytoplasm area was detected using area of Draq5 emission at 640 nm or cell mask at 640 nm. Virus-specific antigen was quantified by measuring the fluorescence emission of DyLight at 488 nm in cytoplasm area of each cell. Acquired images were analyzed using Acapella (Harmony) PE software. Cells that exhibited antigen signal higher than the selected threshold were counted as positive for viral infection. The ratio of virus-positive cells to the total number of analyzed cells was used to determine the percentage of infection for each well in the assay plates. The effect of peptide inhibitors on viral infection was assessed using Genedata software and was calculated as percent inhibition of infection in comparison to 16 non-infected and 16 infected DMSO-treated control wells on each plate. The resultant % inhibition of infection was calculated for each well and used for the dose–response curve analysis. Multi-parameter regression analysis utilized the Levenberg–Marquardt algorithm for selecting the best model and data point exclusion. R^2 value quantified goodness of fit and the fitting strategy was considered acceptable at $R^2 > 0.8$.

2.7. Entry assay (Radoshitzky et al., 2011)

HEK 293T cells were transfected with plasmids encoding EBOV-May GP1,2-(Δ309–489), pQCXIX vector (Clontech) expressing green fluorescent protein (GFP), and plasmid encoding the Moloney murine leukemia virus (MoMLV) gag and pol genes using the calcium-phosphate method and equal concentrations of each plasmid. Forty-eight hours later cell supernatants were cleared of cellular debris by centrifugation and filtration. For the transduction assay, HeLa cells were seeded in a 96-well plate one day before the assay (7000 cells per well). Peptides were added to the cells at the indicated concentrations and incubated at 37 °C for 1 h. Cells incubated with no peptides or with DMSO alone served as controls. Supernatants containing MoMLV-EBOV $GP_{1,2}$ pseudotypes were added to the cells. After 6 h incubation at 37 °C, pseudotypes and peptides were removed and cells were washed 3 times with PBS and supplemented with fresh growth media. One day later, cells were fixed and stained with Hoechst and CellMask. Entry rates were determined by high-content imaging (based on percentage of GFP-positive cells).

2.8. Mouse challenge study

The *in vivo* efficacy of peptides EBOV-5 through −8 was evaluated using the rodent EBOV model in BSL-4 containment facilities at USAMRIID. Six to 12-week old BALB/C mice (Charles River Laboratories) (n = 10 per group) were infected via intraperitoneal injection with 1000 plaque-forming units (pfu) of mouse-adapted EBOV variant Mayinga beginning on Study Day 0. Peptides were formulated in 5% DMSO in PBS and administered at a dose of 10 mg/kg by subcutaneous (SC) injection twice-daily (BID, 20 mg/kg/day) for a total of 9 days. Treatment was initiated shortly after infection on Day 0. The control group was administered vehicle only (5% DMSO in PBS) in a volume equivalent to that of the peptides (200 μL). Following EBOV exposure, animals were observed at least twice-daily for clinical signs of disease. To obtain animal weights, the group weight of all surviving animals within a treatment cohort was measured daily during the first

observation of the day. Animals were humanely euthanized when deemed moribund or at the end of the in-life phase (Study Day 14), using CO_2 inhalation followed by cervical dislocation. Kaplan-Meyer survival analysis and percent changes in weight were generated using GraphPad software (version 6.04).

3. Results

3.1. Cholesterol-conjugated inhibitors

The starting point for design was the HR2-derived inhibitor reported by Higgins et al. (2013). The peptide spans the sequence 610–633 of EBOV GP_2, with a GSGKKK linker between the viral sequence and Cys-conjugated cholesterol. The authors explored N- (1-chol) and C-terminal (2-chol) conjugation. When evaluated against pseudotyped vesicular stomatitis virus particles bearing the EBOV glycoprotein (VSV-GP), the peptides inhibited viral entry with an $IC_{50} < 10\,\mu M$. However, the N-terminally conjugated peptide was unexpectedly more potent than the C-terminal conjugate, in contrast with the expected directionality of the HR1-HR2 domains in the fusion intermediate, as well as the results for most other fusion inhibitors (Ingallinella et al., 2009; Mathieu et al., 2017). Moreover, there was a non-specific component to activity, since some inhibition of native VSV particles was observed for both peptides (Higgins et al., 2013). To establish if the sequence of Higgins et al. was a bona fide EBOV inhibitor of infection of authentic virus, we prepared EBOV-1 (Table 1), a C-terminally conjugated peptide which has the same sequence but lacks the linker GCGKKK; instead, we used a PEG_4 spacer between Cys and the cholesterol group (Augusto et al., 2014; Lee et al., 2011; Mathieu et al., 2017; Porotto et al., 2010a; Welsch et al., 2013).

An important lesson learned from HIV fusion inhibitors is the importance of the regions upstream and downstream of the helical HR2 domain, which contribute to the stability of the complex with the N-terminal HR domain, and hence to the potency of the corresponding fusion inhibitor. In HIV, the region downstream of the HR2 domain, known as the membrane external proximal region (MEPR), is a critical part of enfuvirtide, while the region upstream of HR2 contributes to potency of the second-generation fusion inhibitor sifuvirtide, currently in late-stage clinical trials (He et al., 2008; Yao et al., 2012).

Peptides EBOV-2 and EBOV-3 (Table 1) explored the effect of the addition of the upstream and downstream regions, respectively, of Ebola GP_2 on the inhibitory potency of the HR2 peptide. Since the upstream region contains three cysteine residues, these were substituted with 2-aminobutyric acid (Abu, U), a cysteine isostere.

As shown in Table 2, while EBOV-1 and -2 did not show appreciable inhibition of EBOV infection when used at concentrations up to 30 μM, EBOV-3 inhibited infection with an $EC_{50} = 12.4\,\mu M$. Notably, the peptide also inhibited infection with MARV and SUDV, with comparable potency (Table 2). Therefore similar to HIV, the MPER of filoviruses contributes to the stability of the post-fusion structure and is an important component of a fusion inhibitor. These peptides were also tested in a CHIKV infection assay and did not show any inhibition (data not shown), confirming the absence of any non-specific antiviral effects. Additional tests of these peptides using a second cell line (HFF) with EBOV infection confirmed that there is no dependence of the antiviral effect of the peptides on the cellular background (data not shown).

3.2. Cholesterol-conjugated stapled inhibitors

Short synthetic peptides, like those corresponding to the helical region of the HR2 domain of EBOV, are usually not thermodynamically stable helices in water and rather adopt a random structure (Scholtz and Baldwin, 1992). Preforming the α-helical structure would reduce the entropic cost for binding and increase the affinity for the receptor; accordingly, various strategies have been employed to bias the peptide backbone toward the desired conformation. These include the introduction of unnatural amino acids, noncovalent side chain interactions, and covalent side chain linkers (de Araujo et al., 2014) such as disulfide (Leduc et al., 2003), hydrazine (Calvo et al., 2003), S-alkyl (Fairlie and Dantas de Araujo, 2016), aliphatic (Kim et al., 2011), and lactam bridges (Taylor, 2002). The latter two modifications have been particularly successful in stabilizing virus-derived sequences (Bird et al., 2010, 2014a, 2014b; Harrison et al., 2010; Shepherd et al., 2006). For respiratory syncytial virus (RSV), a 35-residue peptide with two hydrocarbon staples, derived from the HR2 domain of the fusion protein F, was highly helical, stable to protease digestion, and inhibited infection by RSV laboratory isolates in cells and upon mucosal delivery in a mouse model (Bird et al., 2014a). More recently, a shorter bis-stapled RSV peptide, 20-aa in length, was described that inhibits RSV infection in mice upon intranasal administration (Gaillard et al., 2017).

The work of Fairlie and co-workers has shown that the introduction of two back-to-back Lys(*i*)-Asp(*i* + *4*) lactam bridges can enforce a fully α-helical structure with exceptional stability and resistance to denaturation and enzymatic degradation (Fairlie and Dantas de Araujo, 2016; Harrison et al., 2010; Shepherd et al., 2005). For RSV, a bis-lactam stabilized peptide from the HR2 domain of fusion protein, as short as 13 amino acids, showed antiviral potency with $IC_{50} = 36\,nM$, while its linear counterpart was inactive (Shepherd et al., 2006). Optimization of the sequence led to a bis-lactam 12-mer with $IC_{50} = 190\,pM$ (Harrison et al., 2010).

The fact that the bis-lactam constraint is effective for short sequences makes it particularly attractive for EBOV, since the helical segment of the HR2 domain of GP_2 is only 16 amino acids in length. Fig. 1 shows the α-helical region of the HR2 domain of the EBOV GP_2 fusion protein, with the chosen position of the two Lys(*i*)-Asp(*i* + *4*) lactam bridges: Lys^{620}–Asp^{624} and Lys^{625}–Asp^{629}. These positions are not in contact with the HR1 trimer, hence the presence of the lactam should not interfere with HR1-HR2 binding.

In both cases, an Asp residue as required by the Lys(i)–Asp(i + 4) lactam is naturally present at the (i + 4) position: Asp^{624} and Asp^{629}. According to Harrison et al. these side-chain negative charges are engaged in unfavorable electrostatic interactions in the post-fusion structure: (i) an intra-helical *i* – *i* + *3* interaction between Asp^{621} and Asp^{624}, which could destabilize the HR2 α-helix formation at neutral

Table 1
Peptides used in this study.

Peptide	ID	Sequence[1]
EBOV-1	EB-01	IEPHDWTKNITDKIDQIIHDFVDK-C(PEG_4-Chol)
EBOV-2	EB-02	WGGTUHILGPDUUIEPHDWTKNITDKIDQIIHDFVDK-C(PEG_4-Chol)
EBOV-3	EB-03	IEPHDWTKNITDKIDQIIHDFVDKTLPDQG-C(PEG_4-Chol)
EBOV-4	EB-11	DWTKNI**K**DKI**D****K**IIH**D**FVDK-C(PEG_4-Chol)
EBOV-5	EB-12	DWTKNI**K**DKI**D****K**IIH**D**FVDKTLPDQG-C(PEG_4-Chol)
EBOV-6	EB-13	DWTKNI**K**DKI**D****K**IIH**D**FVDKTLPDQG-C(PEG_{12}-Chol)
EBOV-7	EB-14	IEPHDWTKNI**K**DKI**D****K**IIH**D**FVDKTLPDQG-C(PEG_{12}-Chol)
EBOV-8	EB-15	IGIEDLSKNI**K**DKI**D****K**IIH**D**FVDKTLPDQG-C(PEG_{12}-Chol)

[1]All peptides N-terminal acetyl, C-terminal carboxyamide; PEG, polyethylene glycol, n = number of repetitive units; Chol, cholesterol; U = Abu = 2-aminobutyric acid; Bold, underlined: residue engaged in side-chain to side-chai lactam. The two consecutive lactam bridges are indicated in red and blue, respectively.

Table 2
In vitro antiviral activity of cholesterol-conjugated peptides.

Peptide	EBOV EC_{50} [μM]	EBOV EC_{90} [μM]	MARV EC_{50} [μM]	MARV EC_{90} [μM]	SUDV EC_{50} [μM]	SUDVEC_{90} [μM]	CHIKV EC_{50} [μM]	CC_{50} [μM]
EBOV-1	> 30	–	–	–	–	–	–	> 30
	> 30	–	–	–	–	–	–	> 30
EBOV-2	> 30	–	–	–	–	–	–	> 30
	> 30	–	–	–	–	–	–	> 30
EBOV-3	12.89 ± 1.59	–	10.84 ± 1.01	–	16.10 ± 1.63	–	–	> 30
	11.94 ± 2.59	–	10.40 ± 0.97	–	13.09 ± 1.44	–	–	> 30
EBOV-4	6.29 ± 0.66	–	–	–	–	–	–	> 30
	8.10 ± 0.63	–	–	–	–	–	–	> 30
	6.67 ± 0.89	19.41	6.21 ± 0.71	20.52	3.02 ± 0.61	13.63	> 30	> 30
	9.04 ± 1.23	24.79	8.13 ± 0.96	31.30	4.94 ± 1.10	25.03	> 30	> 30
EBOV-5	3.88 ± 0.67	17.27	9.64 ± 0.99	24.74	1.18 ± 0.26	7.05	> 100	> 30
	3.89 ± 0.61	16.86	11.54 ± 1.50	31.38	1.67 ± 0.22	6.87	> 100	> 30
EBOV-6	1.90 ± 0.39	9.84	6.46 ± 0.93	17.03	0.72 ± 0.14	1.58	> 30	> 30
	3.67 ± 0.89	15.33	9.80 ± 0.94	17.59	1.31 ± 0.30	4.49	22.92 ± 2.62	> 30
	5.44 ± 0.85	25.75	–	–	–	–	–	> 25
EBOV-7	1.90 ± 0.28	9.44	–	–	–	–	–	> 25
EBOV-8	18.47 ± 4.64	69.49	–	–	–	–	–	> 25

Antiviral activities of the various EBOV peptides against EBOV, MARV, SUDV, or CHIKV *in vitro*. Cells were inoculated with peptides 2 h prior to virus inoculation. Relative infection rates were determined via immunostaining and high-content quantitative image-based analysis. Results are normalized to DMSO-treated samples. Each value represents results of an independent dose response assay with at least 3 replicates per dose.

pH, due to repulsion between the carboxylate anions, and (ii) an inter-helical repulsive interaction between Glu^{564} of the HR1 and Asp^{629} of the HR2, which may disrupt the inter-helical association at neutral pH (Harrison et al., 2011). Accordingly, pH affects the stability of the 6-helix α-helical bundle of EBOV, with T_m differing by 37 °C between pH 6.1 (T_m = 49.8 ± 1.1 °C) and pH 5.2 (T_m = 86.8 ± 2.0 °C) (Harrison et al., 2011). Hence, removal of the $Asp^{624,629}$ negative charges was likely to be beneficial to inhibitor binding.

The N-terminus of the peptide was chosen at Asp^{614}, since Asp is a good α-helix N-cap (Aurora and Rose, 1998). To further facilitate formation of the helical structure and increase protection against enzymatic degradation, the N-terminus was acetylated and the C-terminus was amidated. Amino acids 631–633 were included in the inhibitor, since they are likely in contact with the HR1 trimer, despite not being visible in the x-ray structure. Moreover, they would contribute two charges that should favor aqueous solubility. The cysteine residue required for cholesterol conjugation was linked directly C-terminal to Lys^{633}. The resulting sequence of EBOV-4 is shown in Table 1 and Fig. 1.

The antiviral activity of the peptide is shown in Table 2. Despite being considerably shorter than EBOV-3 (20 vs. 30 residues), EBOV-4 was found to inhibit all three viruses (EBOV, MARV, and SUDV) more effectively, validating the helix-stabilization strategy. To combine the advantage of a stabilized helical domain with the additional interactions of the MPER domain seen in EBOV-3, we prepared EBOV-5 that includes residues Thr^{634}-Gly^{639}. To explore the optimal distance between the peptide and the cholesterol moieties, the inhibitor EBOV-6 was also constructed, which differs from EBOV-5 only in the length of the PEG spacer (12 vs. 4 units, Table 1). A recent study demonstrated that optimization of the PEG spacer may increase potency (Mathieu et al., 2017). Both peptides were equipotent against EBOV and were slightly more potent than EBOV-4 against EBOV and SUDV, and comparably potent against MARV (Table 2). The equipotent nature of EBOV-5 and EBOV-6 against multiple filoviruses suggest that potency is not impacted by PEG spacers that range between 4 and 12 units. Importantly, peptides EBOV-4, -5, and -6 were also tested in a CHIKV infection assay and were inactive (Table 2), confirming the absence of any non-specific antiviral effects.

Accordingly, the two follow-on peptides EBOV-7 and EBOV-8 (see below) were both prepared with a PEG_{12} spacer. The relatively modest gain in potency conferred by introduction of the MPER region into the bis-lactam inhibitor EBOV-4 suggested that the upstream region missing

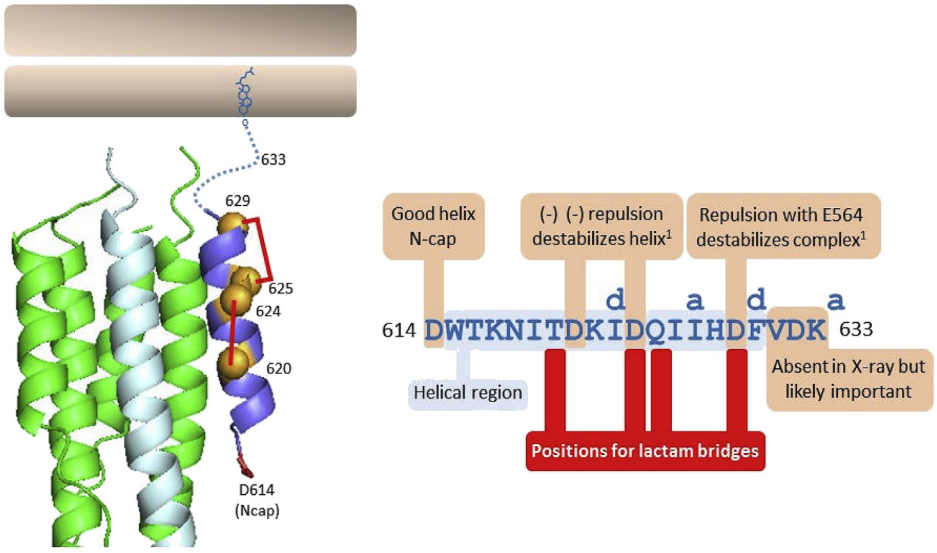

Fig. 1. Design of a helix-stabilized cholesterol-conjugated inhibitor. (Left) The α-helical region of the HR2 domain of Ebola GP_2 in the post-fusion structure (PDB code: 2EBO) is shown with the residues involved in the Lys(i)–Asp(i + 4) lactam bridges as orange spheres in the position of the α-carbon; also indicated are residue Asp^{614}, which N-caps the helix, and the C-terminal residue Lys^{633}, which does not appear in the x-ray structure. (Right) Schematic representation of the design criteria. For full explanation see text.

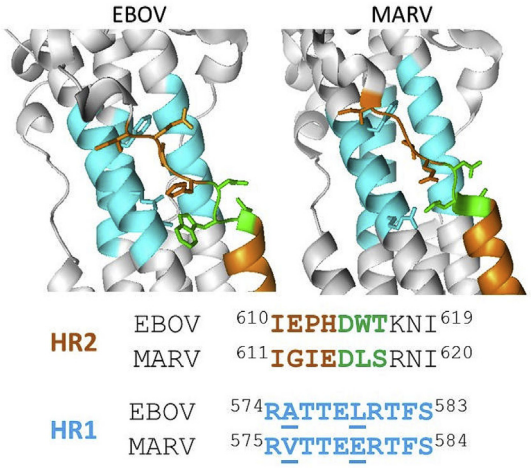

Fig. 2. The region upstream the helix cap in Ebola and Marburg post-fusion structures. The four amino acids (orange) upstream of the helix cap (green) differ between EBOV and MARV, but interact with an identical HR1 surface (cyan). The HR1 residues that differ between EBOV and MARV, Ala^{575}/Val^{576} and Leu^{579}/Glu^{580}, are not part of the surface in contact with HR2.

in EBOV-4 but present in EBOV-3 might be important. Since EBOV-4 is equally active against EBOV and MARV, we expanded our analysis to include the post-fusion structure of MARV GP2 (Harrison et al., 2012; Koellhoffer et al., 2012).

The helical region of HR2 of both EBOV and MARV terminates with a helix cap: for EBOV, the helix is terminated by the Asp^{614}-Trp^{615}-Thr^{616} motif, with the Trp^{615} side-chain closing the HR1 hydrophobic pocket. The correct orientation of Trp^{615} is maintained through the H-bond interaction between Asp^{614} – Thr^{616}; in MARV, the helix cap motif is Asp^{615}-Leu^{616}-Ser^{617}. The Leu^{616} side-chain is positioned like Trp^{615} in EBOV, and the correct orientation of Leu^{616} is maintained through the H-bond interaction between Asp^{615} – Ser^{617} (Fig. S1). Also, the four HR2 amino acids upstream of the helix cap differ between EBOV and MARV (Ile^{610}-Glu-Pro-His^{613} and Ile^{611}-Gly-Ile-Glu^{614}, respectively). However, the whole region interacts with an identical HR1 surface (Fig. 2). Fig. 2 shows an alignment of the interacting HR1 and HR2 regions for EBOV and MARV: the HR1 sequence is conserved, save for Ala^{575}/Val^{576} and Leu^{579}/Glu^{580}, which are not part of the surface in contact with HR2. Therefore, the HR2 sequence 610–616 of EBOV and 611–617 of MARV may represent two binding solutions to the *same* surface. To establish which was the optimal one we generated peptide EBOV-7, including the 4-aa upstream extension, and peptide EBOV-8, in which the entire sequence $GP_2^{611\text{-}617}$ of MARV including the helix cap was grafted into the EBOV backbone (Table 1). The results shown in Table 2 indicate that for ebolavirus the EBOV sequence represents the best binding solution, with EBOV-7 being much more potent than EBOV-8. EBOV-8 is also less potent than EBOV-13; suggesting that the helix cap of the MARV sequence is less effective than the corresponding helix cap of EBOV, at least when transplanted into the EBOV HR2.

Overall, the addition of the four amino acids upstream of the helical domain provides a comparable, modest increase in potency to the addition of the five residues downstream, with EBOV-7 being 2-fold more potent than EBOV-6 and 4-fold more potent than EBOV-4 (Table 2). Peptides EBOV-5 to EBOV-8 were subsequently evaluated for inhibition of viral entry using a previously described assay that utilizes retroviral pseudotypes of EBOV and MARV glycoproteins (Radoshitzky et al., 2011) (Table 3). For EBOV, the results in this assay parallel those in the infectivity assay, with EBOV-7 being the most potent inhibitor of EBOV-GP mediated entry, followed by EBOV-6 and EBOV-5. EBOV-8, with the N-terminal 7-aa from MARV instead of EBOV, was the least potent of all four peptides that were tested.

For Marburg virus, EBOV-6 and EBOV-8 showed comparable

Table 3
Inhibition of EBOV and MARV GP-pseudotyped retrovirus cellular entry by cholesterol-conjugated peptides.

Peptide	EBOV-GP EC_{50} (μM)	EBOV-GP EC_{90} (μM)	MARV-GP EC_{50} (μM)	MARV-GP EC_{90} (μM)	CC_{50} (μM)
EBOV-5	2.45 ± 1.09	29.46	6.20 ± 1.38	25.58	≥25
EBOV-6	1.82 ± 0.55	29.46	3.99 ± 0.87	19.84	≥25
EBOV-7	0.60 ± 0.20	6.15	8.45 ± 1.49	33.36	≥25
EBOV-8	4.02 ± 1.13	20.22	4.66 ± 0.59	15.13	≥25

HeLa cells were inoculated with peptides 2 h prior to pseudotype inoculation. Cells were transduced with enhanced green fluorescent protein (eGFP)-expressing MoMLV pseudotyped with the envelope proteins ($GP_{1,2}$) of EBOV or MARV. eGFP-expressing cells were measured as in Table 2. Results are normalized to DMSO-treated samples. Each value represents results of an independent dose response assay with at least 3 replicates per dose.

inhibition of MARV-GP mediated entry, while EBOV-5 and EBOV-7 were slightly less potent. Together with the results of the infectivity assay, these data suggest that hybridization of the EBOV and MARV sequence may not be a preferred strategy to develop a pan-filovirus inhibitor.

Peptides EBOV-5 to EBOV-8 were then tested for inhibition of EBOV infection in the context of an *in vitro* rodent cellular model. The infection of rodent BHK-21 cells with mouse-adapted EBOV (ma-EBOV) variant Mayinga was used to help translate and correlate antiviral activity between human and rodent cellular models. As shown in Table 4, potency values followed earlier trends shown in Tables 2 and 3 The EBOV-targeting peptides (EBOV-5, -6, and -7) range in potency between 0.5 μM for the most potent peptide (EBOV-7) and as low as 8 μM for the least potent peptide (EBOV-6). The MARV/EBOV targeting peptide (EBOV-8) was less robust against ma-EBOV as well.

3.3. Mouse Pharmacokinetics of EBOV-5 and EBOV-6

The pharmacokinetics of EBOV-5 and EBOV-6 were studied in Balb/c mice, the same strain that was planned for the mouse protection study (Fig. 3). Both peptides exhibited prolonged circulation in plasma, being detectable after 24h upon subcutaneous (SQ) or intravenous (IV) injection at 2-10 mg/kg. The dose-AUC relationship was linear for EBOV-5 but less than linear for EBOV-6. At 10 mg/kg EBOV-5 (Fig. 3a), featuring a 4-unit PEG spacer, reached higher peak and trough concentrations than EBOV-6 (Fig. 3b), featuring a 12-unit PEG spacer. The Cmax and AUC0-24 were 23,000 ng/mL (5.96 μM) and 384,000 ng/mL/h (99.33 μM/h) for EBOV-5 and 14,700 (3.48 μM) and 231,000 ng/mL (54.76 μM/h) for EBOV-6. At 10 mg/kg, EBOV-5 and EBOV-6 maintain a plasma concentration higher than the respective EC50 for 12h. It was therefore decided to administer the peptides at this concentration twice daily (BID), for a total of 20 mg peptide/kg/day.

Table 4
Antiviral activity of cholesterol-conjugated peptides in rodent cells infected with mouse-adapted EBOV.

Peptide	ma-EBOV EC_{50} (μM)	ma-EBOV EC_{90} (μM)	CC_{50} (μM)
EBOV-5	2.34 ± 0.69	16.2	≥51.7
EBOV-6	7.95 ± 28.30	211	≥47.4
EBOV-7	0.50 ± 0.09	3.45	≥42.6
EBOV-8	19.80 ± 1953	142	≥44.0

Antiviral activities of selected EBOV peptides against mouse-adapted (ma-EBOV) *in vitro*. BHK cells were inoculated with peptides 2 h prior to virus inoculation. Relative infection rates were determined as in Table 2. Results are normalized to DMSO-treated samples. Each value represents results of an independent dose response assay with at least 3 replicates per dose.

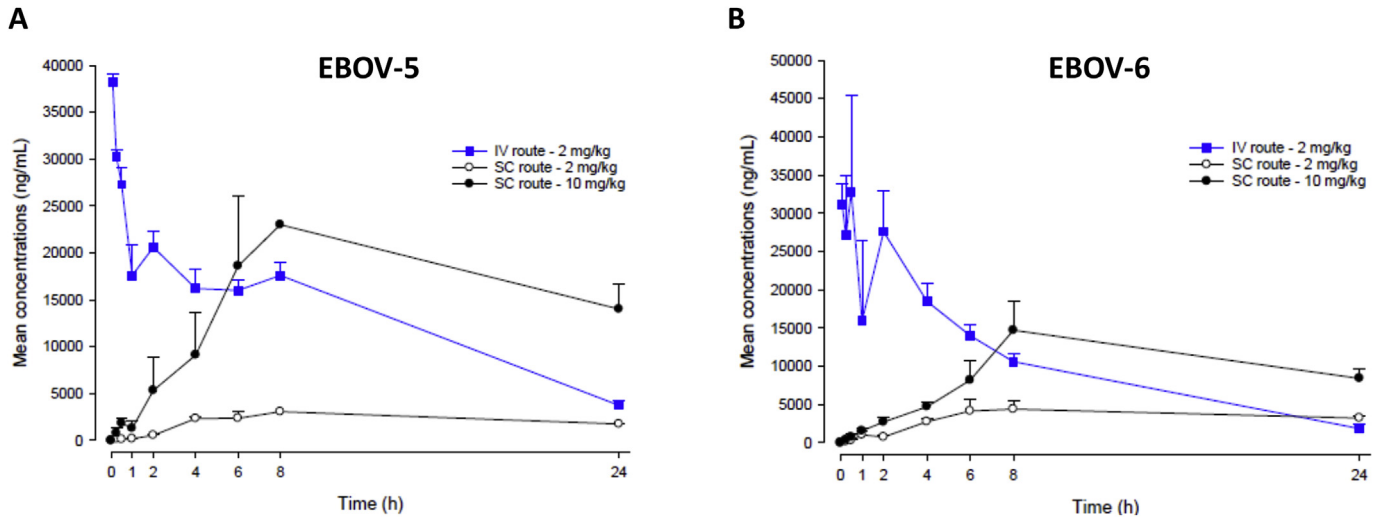

Fig. 3. Pharmacokinetic profiles of EBOV-5 and EBOV-6 peptides in BALB/c mice. Peptides were parenterally administered to mice (n = 3/group) at 2 mg/kg by the intravenous and subcutaneous routes or at 10 mg/kg subcutaneously as indicated by the key for A) EBOV-5 and B) EBOV-6. A plasma concentration curve of 1μM corresponds to 3,865 ng/mL and 4,218 ng/mL for EBOV-5 and EBOV-6, respectively.

3.4. Inhibition of EBOV infection in vivo

The four most potent inhibitors, EBOV-5 to −8, were tested in a mouse model of Ebola virus infection (Bray et al., 1998). The model utilizes a mouse-adapted EBOV variant Mayinga that is lethal for mature, immunocompetent BALB/c inbred mice, with pathologic changes in the liver and spleen resembling those in EBOV-infected non-human primates. Each peptide was administered as a 10 mg/kg SC injection BID (20 mg/kg/day) for 9 days beginning on Study Day 0. The animals were infected intraperitoneally (IP) with 1000 pfu of ma-EBOV and monitored for 14 days. The results of the study are shown in Fig. 4. In the initial study (Fig. 4a), six of the control mice succumbed to infection between Study Days 5–8, with four animals surviving until Day 14 (40% survival, which is significantly more than the typical 100% mortality normally seen in this model). In the treated groups, EBOV-7 was the only peptide to provide statistically significant protection against lethal EBOV infection. Survival in the animals administered EBOV-7 SC BID was 100% (P = 0.0042 by Log-Rank analysis). Survival for EBOV-5, EBOV-6, and EBOV-8 was 60%, 40%, and 30%, respectively, and was comparable to the survival in the control group (Fig. 4a). As expected, weight loss resulting from EBOV infection was observed from Study Days 4–8, with all surviving animals regaining

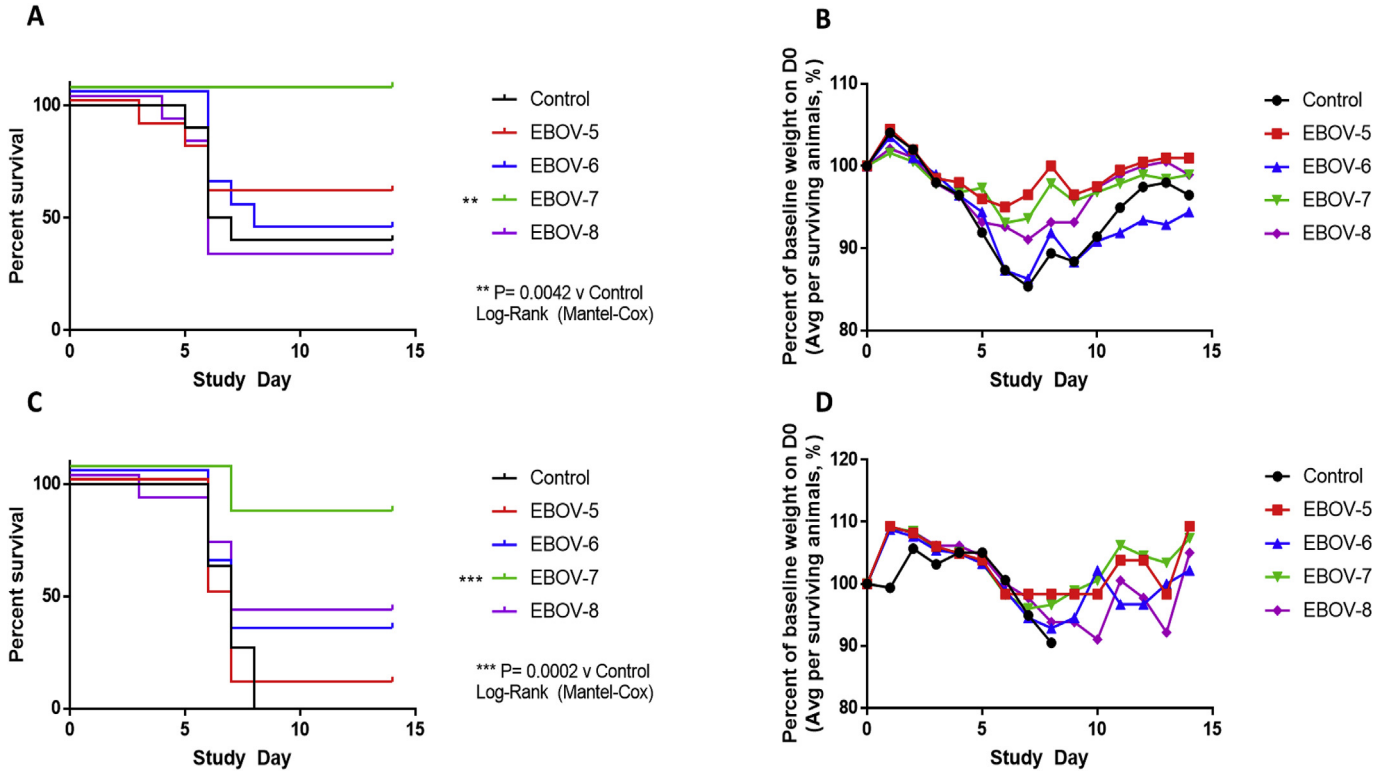

Fig. 4. Inhibition of mouse-adapted EBOV infection in BALB/c mice (n = 10/group) treated with the indicated peptides at 10 mg/kg twice daily (BID). Survival curves from two independent studies are shown in (a) and (c), with the percent change in weight for each group shown in (b) and (d).

weight after Day 8. Weight loss was reduced with respect to the control group in the mice treated with EBOV-5, EBOV-7, and EBOV-8, but not EBOV-6 (Fig. 4b).

To ensure performance of the model, which typically results in near-uniform lethality in control animals, a second iteration of the study was performed. In this iteration, all control mice succumbed to infection between Study Days 6–9 (0% survival) (Fig. 4c). EBOV-7 remained the strongest performer of the four peptides, with 80% survival ($P = 0.0002$ by Log-Rank analysis). Survival for the three remaining peptides (EBOV-5, -6, and -8) ranged from 10 to 40% and was not statistically different from survival in the control group. Similar general trends in weight loss were observed in this iteration (Fig. 4d) as compared to the initial study (Fig. 4b).

4. Discussion

The development of fusion inhibitors for viruses that undergo fusion with intracellular compartments is considerably more challenging than for viruses that fuse at the surface of the cell. This is because of the additional requirement for the inhibitor to reach the endosomal compartments where fusion occurs. Accordingly, the reported potency of HR2-derived peptides from the intracellularly-fusing viruses (e.g., influenza virus (Lee et al., 2011), EBOV (Higgins et al., 2013; Miller et al., 2011)) and extracellularly-fusing viruses (e.g., HIV (Ingallinella et al., 2009), Hendra virus (Porotto et al., 2006), Nipah virus (Porotto et al., 2010b), RSV (Lambert et al., 1996)) differ more than 100-fold. Therefore, several strategies must be applied to generate inhibitors of sufficient potency to approach a clinical candidate. Here we report the combination of cholesterol conjugation with stapling, i.e. the introduction of side-chain to side-chain constraints to stabilize a helical structure in peptides derived from the HR2 domain of EBOV GP_2.

The first strategy utilized is cholesterol conjugation. Cholesterol conjugation increases antiviral activity by targeting the inhibitor to lipid rafts where fusion occurs (Ingallinella et al., 2009; Pessi, 2015). This effect has been exploited by Higgins et al. who described an inhibitor with $IC_{50} < 10\,\mu M$ in a VSVG-Ebola GP pseudovirus assay (Higgins et al., 2013). Using an infection assay with authentic EBOV, we could not confirm this result (peptide EBOV-1, Tables 1 and 2). However, a peptide elongated with the five residues downstream of the helical domain was active, with an IC_{50} of $12\,\mu M$ against EBOV infection (EBOV-3, Tables 1 and 2). The differences between the two assays might explain the discrepancy.

Cholesterol conjugation also provides an improvement in the PK of the peptide (Ingallinella et al., 2009). We confirmed this for the two peptides analyzed here, EBOV-5 and -6 (Table 3), which both were suitable for BID or potentially once-daily administration in mice. The cumulative evidence from the literature (Ingallinella et al., 2009; Li et al., 2013; Mathieu et al., 2017; Porotto et al., 2010a) suggests that a favorable PK profile can be expected for *any* cholesterol-conjugated peptide; accordingly EBOV-7, which we did not analyze for PK, was effective in mice upon BID administration.

The second strategy used is stapling, to pre-form the α-helical structure of the HR2 domain and reduce the entropic cost for binding. Among the many available solutions, we chose to introduce two back-to-back lactam bridges as described by Fairlie and colleagues (Harrison et al., 2010; Shepherd et al., 2005, 2006). The contribution of helix stabilization can be assessed through comparison of EBOV-3 and EBOV-7, which have the same sequence and differ only by the presence of the double staple of EBOV-7, which is more potent by 10-fold (Table 2). This enhancement in potency is less pronounced than that of RSV antivirals in the literature (Bird et al., 2014a; Gaillard et al., 2017; Harrison et al., 2010). The different fusion sites of the viruses (RSV fuses with the cell membrane whereas EBOV fuses with intracellular endo-lysosomal membranes) may also be a contributing factor in this case. However, it is equally, if not more likely, that the details of how stapling is optimally achieved are specific to each virus. For RSV, varying the type and position of the side-chain constraints (Gaillard et al., 2017) had a considerable impact on activity, in agreement with other literature examples (Hojo et al., 2016). Indeed, in addition to stabilizing the secondary structure, the staple may interact with the target protein and provide additional binding energy (Tan et al., 2016). This provides a potential roadmap for evolution of the current peptides.

The most potent peptide, EBOV-7, resulted from the combination of stapling with cholesterol conjugation and was able to protect mice from lethal EBOV infection. In the same study, three other peptides were tested, but they did not provide statistically significant protection from virus infection. Given the small difference in *in vitro* potency, especially with EBOV-6, protection likely depends on reaching a threshold of plasma AUC and EC_{50}, with a slight decline in either parameter contributing to the lack of protection in this *in vivo* model.

In this respect, optimization of the PEG linker may provide a major benefit, since it simultaneously influences PK and potency (Table 2). A recent study has shown that the optimal length of the PEG spacer may vary between viruses: extending the number of PEG units from 4 to 12 increased potency against Nipah virus, but not against human paramyxovirus (Mathieu et al., 2017). In the same study, extension to 24 PEG units further improved potency (Mathieu et al., 2017). However, in our study we observed a slightly better PK profile for PEG_4 vs PEG_{12} containing peptides (Fig. 3), highlighting the need to consider both parameters.

In summary, we have developed stapled, cholesterol-conjugated fusion inhibitors that are active *in vitro* against both EBOV and MARV and can prevent lethal EBOV infection in a rodent model. These peptides represent promising leads for a filovirus-specific therapeutic.

Competing financial interests

Antonello Pessi was an employee of PeptiPharma, Pascale Vicat and Valerie Couturier were employees of Sanofi (Paris), Kent Kester and John Shiver were employees of Sanofi Pasteur (Swiftwater), and Kara Carter was an employee of Sanofi (Cambridge) while these studies were conducted. The authors have no other declarations of interest.

Disclaimer

Opinions, interpretations, conclusions, and recommendations are those of the authors and are not necessarily endorsed by the U.S. Army. Research was conducted under an IACUC approved protocol in compliance with the Animal Welfare Act, PHS Policy, and other Federal statutes and regulations relating to animals and experiments involving animals. The facility where this research was conducted is accredited by the Association for Assessment and Accreditation of Laboratory Animal Care, International and adheres to principles stated in the Guide for the Care and Use of Laboratory Animals, National Research Council, 2011.

Acknowledgements

We thank Drs. Stewart Hamilton, Tina Nguyen, Stéphanie Henriot, and Gilles Parmentier, for help with the custom synthesis of the peptides. We also acknowledge the critical roles of Julie Tran (USAMRIID Division of Molecular and Translational Sciences) in purification of the monoclonal antibodies used for virus detection and Tim Voloshen (Sanofi Pasteur) for peptide-related logistics.

This work was supported in part by funding from the United States of America provided by The Joint Science and Technology Office for Chemical and Biological Defense (JSTO-CBD) of the Defense Threat Reduction Agency (DTRA) under plan number CB10217. The funding agency had no involvement in any aspect of the study including design, data collection, analysis, interpretation, or composition of this manuscript.

Appendix A. Supplementary data

Supplementary data to this article can be found online at https://doi.org/10.1016/j.antiviral.2019.104592.

References

Aman, M.J., 2016. Chasing ebola through the endosomal labyrinth. mBio 7 e00346.

Augusto, M.T., Hollmann, A., Castanho, M.A., Porotto, M., Pessi, A., Santos, N.C., 2014. Improvement of HIV fusion inhibitor C34 efficacy by membrane anchoring and enhanced exposure. J. Antimicrob. Chemother. 69, 1286–1297.

Aurora, R., Rose, G.D., 1998. Helix capping. Protein Sci. 7, 21–38.

Bird, G.H., Boyapalle, S., Wong, T., Opoku-Nsiah, K., Bedi, R., Crannell, W.C., Perry, A.F., Nguyen, H., Sampayo, V., Devareddy, A., Mohapatra, S., Mohapatra, S.S., Walensky, L.D., 2014a. Mucosal delivery of a double-stapled RSV peptide prevents nasopulmonary infection. J. Clin. Investig. 124, 2113–2124.

Bird, G.H., Irimia, A., Ofek, G., Kwong, P.D., Wilson, I.A., Walensky, L.D., 2014b. Stapled HIV-1 peptides recapitulate antigenic structures and engage broadly neutralizing antibodies. Nat. Struct. Mol. Biol. 21, 1058–1067.

Bird, G.H., Madani, N., Perry, A.F., Princiotto, A.M., Supko, J.G., He, X., Gavathiotis, E., Sodroski, J.G., Walensky, L.D., 2010. Hydrocarbon double-stapling remedies the proteolytic instability of a lengthy peptide therapeutic. Proc. Natl. Acad. Sci. U. S. A. 107, 14093–14098.

Bixler, S.L., Bocan, T.M., Wells, J., Wetzel, K.S., Van Tongeren, S.A., Dong, L., Garza, N.L., Donnelly, G., Cazares, L.H., Nuss, J., Soloveva, V., Koistinen, K.A., Welch, L., Epstein, C., Liang, L.F., Giesing, D., Lenk, R., Bavari, S., Warren, T.K., 2018. Efficacy of favipiravir (T-705) in nonhuman primates infected with Ebola virus or Marburg virus. Antivir. Res. 151, 97–104.

Bornholdt, Z.A., Turner, H.L., Murin, C.D., Li, W., Sok, D., Souders, C.A., Piper, A.E., Goff, A., Shamblin, J.D., Wollen, S.E., Sprague, T.R., Fusco, M.L., Pommert, K.B., Cavacini, L.A., Smith, H.L., Klempner, M., Reimann, K.A., Krauland, E., Gerngross, T.U., Wittrup, K.D., Saphire, E.O., Burton, D.R., Glass, P.J., Ward, A.B., Walker, L.M., 2016. Isolation of potent neutralizing antibodies from a survivor of the 2014 Ebola virus outbreak. Science 351, 1078–1083.

Bray, M., Davis, K., Geisbert, T., Schmaljohn, C., Huggins, J., 1998. A mouse model for evaluation of prophylaxis and therapy of Ebola hemorrhagic fever. J. Infect. Dis. 178, 651–661.

Calvo, J.C., Choconta, K.C., Diaz, D., Orozco, O., Bravo, M.M., Espejo, F., Salazar, L.M., Guzman, F., Patarroyo, M.E., 2003. An alpha helix conformationally restricted peptide is recognized by cervical carcinoma patients' sera. J. Med. Chem. 46, 5389–5394.

Carette, J.E., Raaben, M., Wong, A.C., Herbert, A.S., Obernosterer, G., Mulherkar, N., Kuehne, A.I., Kranzusch, P.J., Griffin, A.M., Ruthel, G., Dal Cin, P., Dye, J.M., Whelan, S.P., Chandran, K., Brummelkamp, T.R., 2011. Ebola virus entry requires the cholesterol transporter Niemann-Pick C1. Nature 477, 340–343.

Chandran, K., Sullivan, N.J., Felbor, U., Whelan, S.P., Cunningham, J.M., 2005. Endosomal proteolysis of the Ebola virus glycoprotein is necessary for infection. Science 308, 1643–1645.

Cote, M., Misasi, J., Ren, T., Bruchez, A., Lee, K., Filone, C.M., Hensley, L., Li, Q., Ory, D., Chandran, K., Cunningham, J., 2011. Small molecule inhibitors reveal Niemann-Pick C1 is essential for Ebola virus infection. Nature 477, 344–348.

Cross, R.W., Mire, C.E., Feldmann, H., Geisbert, T.W., 2018. Post-exposure treatments for Ebola and Marburg virus infections. Nat. Rev. Drug Discov. 17, 413–434.

de Araujo, A.D., Hoang, H.N., Kok, W.M., Diness, F., Gupta, P., Hill, T.A., Driver, R.W., Price, D.A., Liras, S., Fairlie, D.P., 2014. Comparative alpha-helicity of cyclic pentapeptides in water. Angew Chem. Int. Ed. Engl. 53, 6965–6969.

Eckert, D.M., Kim, P.S., 2001. Mechanisms of viral membrane fusion and its inhibition. Annu. Rev. Biochem. 70, 777–810.

Fairlie, D.P., Dantas de Araujo, A., 2016. Review stapling peptides using cysteine crosslinking. Biopolymers 106, 843–852.

Feldmann, H., Geisbert, T.W., 2011. Ebola haemorrhagic fever. Lancet 377, 849–862.

Flyak, A.I., Shen, X., Murin, C.D., Turner, H.L., David, J.A., Fusco, M.L., Lampley, R., Kose, N., Ilinykh, P.A., Kuzmina, N., Branchizio, A., King, H., Brown, L., Bryan, C., Davidson, E., Doranz, B.J., Slaughter, J.C., Sapparapu, G., Klages, C., Ksiazek, T.G., Saphire, E.O., Ward, A.B., Bukreyev, A., Crowe Jr., J.E., 2016. Cross-reactive and potent neutralizing antibody responses in human survivors of natural ebolavirus infection. Cell 164, 392–405.

Frei, J.C., Nyakatura, E.K., Zak, S.E., Bakken, R.R., Chandran, K., Dye, J.M., Lai, J.R., 2016. Bispecific antibody affords complete post-exposure protection of mice from both ebola (Zaire) and Sudan viruses. Sci. Rep. 6, 19193.

Furuyama, W., Marzi, A., Nanbo, A., Haddock, E., Maruyama, J., Miyamoto, H., Igarashi, M., Yoshida, R., Noyori, O., Feldmann, H., Takada, A., 2016. Discovery of an antibody for pan-ebolavirus therapy. Sci. Rep. 6, 20514.

Gaillard, V., Galloux, M., Garcin, D., Eleouet, J.F., Le Goffic, R., Larcher, T., Rameix-Welti, M.A., Boukadiri, A., Heritier, J., Segura, J.M., Baechler, E., Arrell, M., Mottet-Osman, G., Nyanguile, O., 2017. A short double-stapled peptide inhibits respiratory syncytial virus entry and spreading. Antimicrob. Agents Chemother. 61 e02241-16.

Gallaher, W.R., 1996. Similar structural models of the transmembrane proteins of Ebola and avian sarcoma viruses. Cell 85, 477–478.

Haque, A., Hober, D., Blondiaux, J., 2015. Addressing therapeutic options for ebola virus infection in current and future outbreaks. Antimicrob. Agents Chemother. 59, 5892–5902.

Harrison, J.S., Higgins, C.D., Chandran, K., Lai, J.R., 2011. Designed protein mimics of the Ebola virus glycoprotein GP2 alpha-helical bundle: stability and pH effects. Protein Sci. 20, 1587–1596.

Harrison, J.S., Koellhoffer, J.F., Chandran, K., Lai, J.R., 2012. Marburg virus glycoprotein GP2: pH-dependent stability of the ectodomain alpha-helical bundle. Biochemistry 51, 2515–2525.

Harrison, R.S., Shepherd, N.E., Hoang, H.N., Ruiz-Gomez, G., Hill, T.A., Driver, R.W., Desai, V.S., Young, P.R., Abbenante, G., Fairlie, D.P., 2010. Downsizing human, bacterial, and viral proteins to short water-stable alpha helices that maintain biological potency. Proc. Natl. Acad. Sci. U. S. A. 107, 11686–11691.

He, Y., Xiao, Y., Song, H., Liang, Q., Ju, D., Chen, X., Lu, H., Jing, W., Jiang, S., Zhang, L., 2008. Design and evaluation of sifuvirtide, a novel HIV-1 fusion inhibitor. J. Biol. Chem. 283, 11126–11134.

Higgins, C.D., Koellhoffer, J.F., Chandran, K., Lai, J.R., 2013. C-peptide inhibitors of Ebola virus glycoprotein-mediated cell entry: effects of conjugation to cholesterol and side chain-side chain crosslinking. Bioorg. Med. Chem. Lett 23, 5356–5360.

Hojo, K., Hossain, M.A., Tailhades, J., Shabanpoor, F., Wong, L.L., Ong-Palsson, E.E., Kastman, H.E., Ma, S., Gundlach, A.L., Rosengren, K.J., Wade, J.D., Bathgate, R.A., 2016. Development of a single-chain peptide agonist of the relaxin-3 receptor using hydrocarbon stapling. J. Med. Chem. 59, 7445–7456.

Holmes, E.C., Dudas, G., Rambaut, A., Andersen, K.G., 2016. The evolution of Ebola virus: insights from the 2013-2016 epidemic. Nature 538, 193–200.

Ingallinella, P., Bianchi, E., Ladwa, N.A., Wang, Y.J., Hrin, R., Veneziano, M., Bonelli, F., Ketas, T.J., Moore, J.P., Miller, M.D., Pessi, A., 2009. Addition of a cholesterol group to an HIV-1 peptide fusion inhibitor dramatically increases its antiviral potency. Proc. Natl. Acad. Sci. U. S. A. 106, 5801–5806.

Kim, Y.W., Grossmann, T.N., Verdine, G.L., 2011. Synthesis of all-hydrocarbon stapled alpha-helical peptides by ring-closing olefin metathesis. Nat. Protoc. 6, 761–771.

Koellhoffer, J.F., Malashkevich, V.N., Harrison, J.S., Toro, R., Bhosle, R.C., Chandran, K., Almo, S.C., Lai, J.R., 2012. Crystal structure of the Marburg virus GP2 core domain in its postfusion conformation. Biochemistry 51, 7665–7675.

Kuhn, J.H., Andersen, K.G., Baize, S., Bao, Y., Bavari, S., Berthet, N., Blinkova, O., Brister, J.R., Clawson, A.N., Fair, J., Gabriel, M., Garry, R.F., Gire, S.K., Goba, A., Gonzalez, J.P., Gunther, S., Happi, C.T., Jahrling, P.B., Kapetshi, J., Kobinger, G., Kugelman, J.R., Leroy, E.M., Maganga, G.D., Mbala, P.K., Moses, L.M., Muyembe-Tamfum, J.J., N'Faly, M., Nichol, S.T., Omilabu, S.A., Palacios, G., Park, D.J., Paweska, J.T., Radoshitzky, S.R., Rossi, C.A., Sabeti, P.C., Schieffelin, J.S., Schoepp, R.J., Sealfon, R., Swanepoel, R., Towner, J.S., Wada, J., Wauquier, N., Yozwiak, N.L., Formenty, P., 2014a. Nomenclature- and database-compatible names for the two Ebola virus variants that emerged in Guinea and the Democratic Republic of the Congo in 2014. Viruses 6, 4760–4799.

Kuhn, J.H., Andersen, K.G., Bao, Y., Bavari, S., Becker, S., Bennett, R.S., Bergman, N.H., Blinkova, O., Bradfute, S., Brister, J.R., Bukreyev, A., Chandran, K., Chepurnov, A.A., Davey, R.A., Dietzgen, R.G., Doggett, N.A., Dolnik, O., Dye, J.M., Enterlein, S., Fenimore, P.W., Formenty, P., Freiberg, A.N., Garry, R.F., Garza, N.L., Gire, S.K., Gonzalez, J.P., Griffiths, A., Happi, C.T., Hensley, L.E., Herbert, A.S., Hevey, M.C., Hoenen, T., Honko, A.N., Ignatyev, G.M., Jahrling, P.B., Johnson, J.C., Johnson, K.M., Kindrachuk, J., Klenk, H.D., Kobinger, G., Kochel, T.J., Lackemeyer, M.G., Lackner, D.F., Leroy, E.M., Lever, M.S., Muhlberger, E., Netesov, S.V., Olinger, G.G., Omilabu, S.A., Palacios, G., Panchal, R.G., Park, D.J., Patterson, J.L., Paweska, J.T., Peters, C.J., Pettitt, J., Pitt, L., Radoshitzky, S.R., Ryabchikova, E.I., Saphire, E.O., Sabeti, P.C., Sealfon, R., Shestopalov, A.M., Smither, S.J., Sullivan, N.J., Swanepoel, R., Takada, A., Towner, J.S., van der Groen, G., Volchkov, V.E., Volchkova, V.A., Wahl-Jensen, V., Warren, T.K., Warfield, K.L., Weidmann, M., Nichol, S.T., 2014b. Filovirus RefSeq entries: evaluation and selection of filovirus type variants, type sequences, and names. Viruses 6, 3663–3682.

LaBonte, J., Lebbos, J., Kirkpatrick, P., 2003. Enfuvirtide. Nat. Rev. Drug Discov. 2, 345–346.

Lambert, D.M., Barney, S., Lambert, A.L., Guthrie, K., Medinas, R., Davis, D.E., Bucy, T., Erickson, J., Merutka, G., Petteway Jr., S.R., 1996. Peptides from conserved regions of paramyxovirus fusion (F) proteins are potent inhibitors of viral fusion. Proc. Natl. Acad. Sci. U. S. A. 93, 2186–2191.

Leduc, A.M., Trent, J.O., Wittliff, J.L., Bramlett, K.S., Briggs, S.L., Chirgadze, N.Y., Wang, Y., Burris, T.P., Spatola, A.F., 2003. Helix-stabilized cyclic peptides as selective inhibitors of steroid receptor-coactivator interactions. Proc. Natl. Acad. Sci. U. S. A. 100, 11273–11278.

Lee, J.E., Fusco, M.L., Hessell, A.J., Oswald, W.B., Burton, D.R., Saphire, E.O., 2008. Structure of the Ebola virus glycoprotein bound to an antibody from a human survivor. Nature 454, 177–182.

Lee, K.K., Pessi, A., Gui, L., Santoprete, A., Talekar, A., Moscona, A., Porotto, M., 2011. Capturing a fusion intermediate of influenza hemagglutinin with a cholesterol-conjugated peptide, a new antiviral strategy for influenza virus. J. Biol. Chem. 286, 42141–42149.

Li, C.G., Tang, W., Chi, X.J., Dong, Z.M., Wang, X.X., Wang, X.J., 2013. A cholesterol tag at the N terminus of the relatively broad-spectrum fusion inhibitory peptide targets an earlier stage of fusion glycoprotein activation and increases the peptide's antiviral potency in vivo. J. Virol. 87, 9223–9232.

Malashkevich, V.N., Schneider, B.J., McNally, M.L., Milhollen, M.A., Pang, J.X., Kim, P.S., 1999. Core structure of the envelope glycoprotein GP2 from Ebola virus at 1.9-A resolution. Proc. Natl. Acad. Sci. U. S. A. 96, 2662–2667.

Mathieu, C., Augusto, M.T., Niewiesk, S., Horvat, B., Palermo, L.M., Sanna, G., Madeddu, S., Huey, D., Castanho, M.A., Porotto, M., Santos, N.C., Moscona, A., 2017. Broad spectrum antiviral activity for paramyxoviruses is modulated by biophysical properties of fusion inhibitory peptides. Sci. Rep. 7, 43610.

Miller, E.H., Harrison, J.S., Radoshitzky, S.R., Higgins, C.D., Chi, X., Dong, L., Kuhn, J.H., Bavari, S., Lai, J.R., Chandran, K., 2011. Inhibition of Ebola virus entry by a C-peptide targeted to endosomes. J. Biol. Chem. 286, 15854–15861.

Misasi, J., Gilman, M.S., Kanekiyo, M., Gui, M., Cagigi, A., Mulangu, S., Corti, D., Ledgerwood, J.E., Lanzavecchia, A., Cunningham, J., Muyembe-Tamfun, J.J., Baxa,

U., Graham, B.S., Xiang, Y., Sullivan, N.J., McLellan, J.S., 2016. Structural and molecular basis for Ebola virus neutralization by protective human antibodies. Science 351, 1343–1346.
Mulherkar, N., Raaben, M., de la Torre, J.C., Whelan, S.P., Chandran, K., 2011. The Ebola virus glycoprotein mediates entry via a non-classical dynamin-dependent macropinocytic pathway. Virology 419, 72–83.
Nanbo, A., Imai, M., Watanabe, S., Noda, T., Takahashi, K., Neumann, G., Halfmann, P., Kawaoka, Y., 2010. Ebolavirus is internalized into host cells via macropinocytosis in a viral glycoprotein-dependent manner. PLoS Pathog. 6 e1001121.
Nyakatura, E.K., Frei, J.C., Lai, J.R., 2015. Chemical and structural aspects of ebola virus entry inhibitors. ACS Infect. Dis. 1, 42–52.
Pessi, A., 2015. Cholesterol-conjugated peptide antivirals: a path to a rapid response to emerging viral diseases. J. Pept. Sci. 21, 379–386.
Porotto, M., Doctor, L., Carta, P., Fornabaio, M., Greengard, O., Kellogg, G.E., Moscona, A., 2006. Inhibition of hendra virus fusion. J. Virol. 80, 9837–9849.
Porotto, M., Rockx, B., Yokoyama, C.C., Talekar, A., Devito, I., Palermo, L.M., Liu, J., Cortese, R., Lu, M., Feldmann, H., Pessi, A., Moscona, A., 2010a. Inhibition of Nipah virus infection in vivo: targeting an early stage of paramyxovirus fusion activation during viral entry. PLoS Pathog. 6 e1001168.
Porotto, M., Yokoyama, C.C., Palermo, L.M., Mungall, B., Aljofan, M., Cortese, R., Pessi, A., Moscona, A., 2010b. Viral entry inhibitors targeted to the membrane site of action. J. Virol. 84, 6760–6768.
Qiu, X., Audet, J., Lv, M., He, S., Wong, G., Wei, H., Luo, L., Fernando, L., Kroeker, A., Fausther Bovendo, H., Bello, A., Li, F., Ye, P., Jacobs, M., Ippolito, G., Saphire, E.O., Bi, S., Shen, B., Gao, G.F., Zeitlin, L., Feng, J., Zhang, B., Kobinger, G.P., 2016. Two-mAb cocktail protects macaques against the Makona variant of Ebola virus. Sci. Transl. Med. 8, 329ra333.
Radoshitzky, S.R., Warfield, K.L., Chi, X., Dong, L., Kota, K., Bradfute, S.B., Gearhart, J.D., Retterer, C., Kranzusch, P.J., Misasi, J.N., Hogenbirk, M.A., Wahl-Jensen, V., Volchkov, V.E., Cunningham, J.M., Jahrling, P.B., Aman, M.J., Bavari, S., Farzan, M., Kuhn, J.H., 2011. Ebolavirus delta-peptide immunoadhesins inhibit marburgvirus and ebolavirus cell entry. J. Virol. 85, 8502–8513.
Saeed, M.F., Kolokoltsov, A.A., Albrecht, T., Davey, R.A., 2010. Cellular entry of ebola virus involves uptake by a macropinocytosis-like mechanism and subsequent trafficking through early and late endosomes. PLoS Pathog. 6 e1001110.
Scholtz, J.M., Baldwin, R.L., 1992. The mechanism of alpha-helix formation by peptides. Annu. Rev. Biophys. Biomol. Struct. 21, 95–118.
Shepherd, N.E., Hoang, H.N., Abbenante, G., Fairlie, D.P., 2005. Single turn peptide alpha helices with exceptional stability in water. J. Am. Chem. Soc. 127, 2974–2983.
Shepherd, N.E., Hoang, H.N., Desai, V.S., Letouze, E., Young, P.R., Fairlie, D.P., 2006. Modular alpha-helical mimetics with antiviral activity against respiratory syncitial virus. J. Am. Chem. Soc. 128, 13284–13289.
Skrip, L.A., Galvani, A.P., 2016. Next steps for ebola vaccination: deployment in non-epidemic, high-risk settings. PLoS Neglected Trop. Dis. 10 e0004802.
Tan, Y.S., Lane, D.P., Verma, C.S., 2016. Stapled peptide design: principles and roles of computation. Drug Discov. Today 21, 1642–1653.
Taylor, J.W., 2002. The synthesis and study of side-chain lactam-bridged peptides. Biopolymers 66, 49–75.
Warren, T.K., Jordan, R., Lo, M.K., Ray, A.S., Mackman, R.L., Soloveva, V., Siegel, D., Perron, M., Bannister, R., Hui, H.C., Larson, N., Strickley, R., Wells, J., Stuthman, K.S., Van Tongeren, S.A., Garza, N.L., Donnelly, G., Shurtleff, A.C., Retterer, C.J., Gharaibeh, D., Zamani, R., Kenny, T., Eaton, B.P., Grimes, E., Welch, L.S., Gomba, L., Wilhelmsen, C.L., Nichols, D.K., Nuss, J.E., Nagle, E.R., Kugelman, J.R., Palacios, G., Doerffler, E., Neville, S., Carra, E., Clarke, M.O., Zhang, L., Lew, W., Ross, B., Wang, Q., Chun, K., Wolfe, L., Babusis, D., Park, Y., Stray, K.M., Trancheva, I., Feng, J.Y., Barauskas, O., Xu, Y., Wong, P., Braun, M.R., Flint, M., McMullan, L.K., Chen, S.S., Fearns, R., Swaminathan, S., Mayers, D.L., Spiropoulou, C.F., Lee, W.A., Nichol, S.T., Cihlar, T., Bavari, S., 2016. Therapeutic efficacy of the small molecule GS-5734 against Ebola virus in rhesus monkeys. Nature 531, 381–385.
Warren, T.K., Wells, J., Panchal, R.G., Stuthman, K.S., Garza, N.L., Van Tongeren, S.A., Dong, L., Retterer, C.J., Eaton, B.P., Pegoraro, G., Honnold, S., Bantia, S., Kotian, P., Chen, X., Taubenheim, B.R., Welch, L.S., Minning, D.M., Babu, Y.S., Sheridan, W.P., Bavari, S., 2014. Protection against filovirus diseases by a novel broad-spectrum nucleoside analogue BCX4430. Nature 508, 402–405.
Wec, A.Z., Nyakatura, E.K., Herbert, A.S., Howell, K.A., Holtsberg, F.W., Bakken, R.R., Mittler, E., Christin, J.R., Shulenin, S., Jangra, R.K., Bharrhan, S., Kuehne, A.I., Bornholdt, Z.A., Flyak, A.I., Saphire, E.O., Crowe Jr., J.E., Aman, M.J., Dye, J.M., Lai, J.R., Chandran, K., 2016. A "Trojan horse" bispecific-antibody strategy for broad protection against ebolaviruses. Science 354, 350–354.
Weissenhorn, W., Carfi, A., Lee, K.H., Skehel, J.J., Wiley, D.C., 1998. Crystal structure of the Ebola virus membrane fusion subunit, GP2, from the envelope glycoprotein ectodomain. Mol. Cell 2, 605–616.
Welsch, J.C., Talekar, A., Mathieu, C., Pessi, A., Moscona, A., Horvat, B., Porotto, M., 2013. Fatal measles virus infection prevented by brain-penetrant fusion inhibitors. J. Virol. 87, 13785–13794.
Yao, X., Chong, H., Zhang, C., Waltersperger, S., Wang, M., Cui, S., He, Y., 2012. Broad antiviral activity and crystal structure of HIV-1 fusion inhibitor sifuvirtide. J. Biol. Chem. 287, 6788–6796.